2000-01-1228

Transition from Combustion to Variable Compression Braking

L. Moklegaard and A. G. Stefanopoulou
University of California, Santa Barbara

J. Schmidt
Mack Trucks, Inc.

ABSTRACT

Commercial Heavy vehicles (CHVs) are an efficient and reliable link between marine, railroad, and air transportation nodes. The vehicle braking power imposes an important constraint in the allowable vehicle speed. The compression brake augments the vehicle retarding power and is currently typically used as an on-off device by experienced drivers. Hardware and software advances allow modulation of the compression brake power through variable valve timing, and thus, enable integration of the compression brake with service brakes. To analyze how much the compression brake affects vehicle speed during braking, we develop a crank angle engine model that describes the intrinsic transient interactions between individual cylinder intake and exhaust gas process, turbocharger dynamics, and vehicle dynamics during combustion and variable brake valve timing. The model is validated using experimental data. Using system identification techniques we develop low-order mean-value models appropriate for control analysis and design.

1. INTRODUCTION

Over the last ten years, there has been a significant improvement of the reliability and efficiency of the commercial heavy vehicle (CHV) powertrain. This transformation is primarily achieved by using lightweight material, by reducing aerodynamic drag and frictional losses, and by using electronic engine controls. Fleets regularly choose diesel engines for their powertrains because they use very lean mixtures of fuel and air. In addition, diesel engines operate without a throttle, which means that no intake manifold vacuum is required. The lack of manifold vacuum allows the piston to "free-wheel" since it does not have to work against the manifold vacuum during the intake stroke. This contributes to the increased fuel economy associated with diesel engines, but on the other hand, it does not provide means for decelerating the moving engine parts. Increase in operational vehicle speed combined with decrease of the natural retarding capabilities in modern powertrains creates challenging braking requirements. Engine and truck manufacturers have responded to the need by developing additional retarding mechanisms.

Compression braking is based on inhibiting fuel injection, altering the existing exhaust valve opening, and, thereby, converting the engine into a compressor. In that mode, the engine acts like a energy sink [2], because the crankshaft kinetic energy is used to compress the air during the compression stroke. Close to top-dead-center (TDC), the compressed air is released to the exhaust manifold or to a storage plenum through an engine valve. The process is depicted in Fig. 1. We call this secondary open-

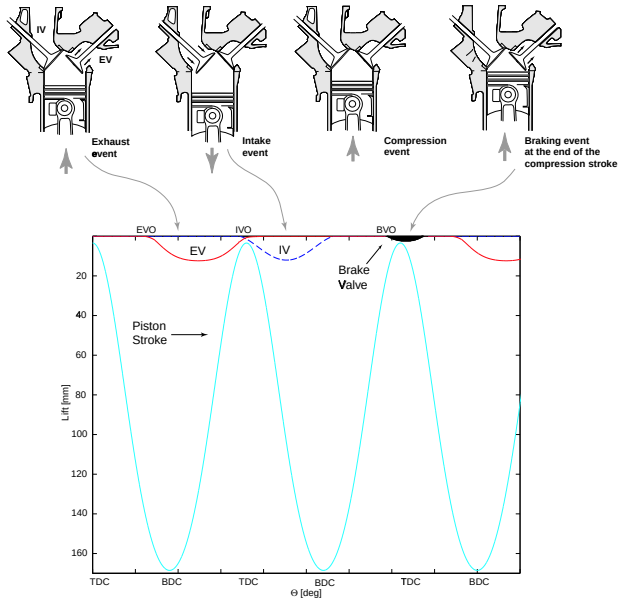

Figure 1: Schematic drawing and traces of piston motion and valve lift profiles.

ing of the exhaust valve the braking event, and the corresponding valve timing for brake valve timing, v_{eb}. In existing systems, such as the ones designed by Jacobs, Pacific Diesel Brake, and Cummins, the exhaust valve is used for both braking and exhaust events. However, the lift profile for the exhaust valve is considerably different for the two events, as shown in Fig. 1. For simplicity, we call the braking event profile of the exhaust valve the "brake valve".

The activation of the brake valve is typically achieved through a master-slave hydraulic system. The exact profile and timing for the brake valve is designed to maximize the braking power, i.e., to generate the highest peak cylinder pressure. Important braking effort limits are imposed by constraints in component loading and clearance between the brake valve and the piston motion.

Fig. 2 illustrates the valve timing events plotted in a **P-V** diagram. This diagram shows the engine operation during conventional 4-stroke cycle operation (dotted line) and the 4-stroke cycle operation during compression braking (solid line). The piston work is positive during conventional combustion mode and negative during compression braking mode. The diagram is generated using outputs from the developed model during steady-state engine conditions. Note here that steady-state conditions are defined in a cycle-averaged sense. The engine is considered at steady-state even though its crank angle based behavior is periodic with one firing or braking cycle as the period.

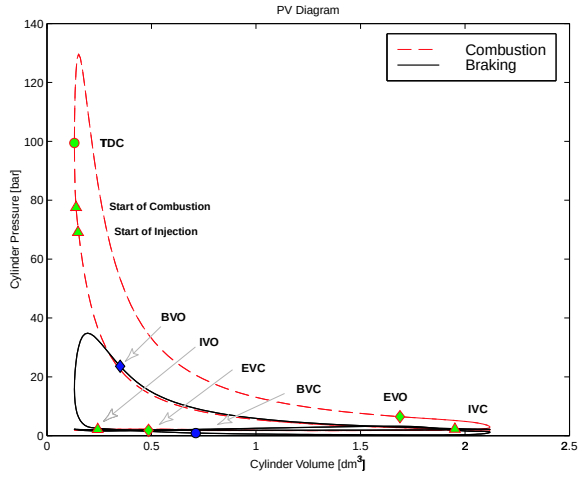

Figure 2: Cylinder pressure versus cylinder volume during combustion (dashed), and braking (solid) mode.

The information attained from Fig. 2 is used in static vehicle stability analysis. Integration of the compression brake with the service brakes is currently addressed only during steady-state operation based on the vehicle characteristics shown in Fig. 3. The figure shows a steady-state map of vehicle kinetic power versus speed during braking on a downhill grade (dashed line). The overall retarding power with (solid line) and without (dash-dot line) compression brake is also shown. The point of intersection of the generated power with the retarding power defines the equilibrium descent speed or vehicle control speed, V_w^*. The existence of an equilibrium speed within the engine safe speed limits demonstrates that a vehicle equipped with a compression brake can proceed down a grade without using service brakes. A vehicle without a compression brake, on the other hand, has to use service brakes to proceed down the grade in a safe and controlled manner.

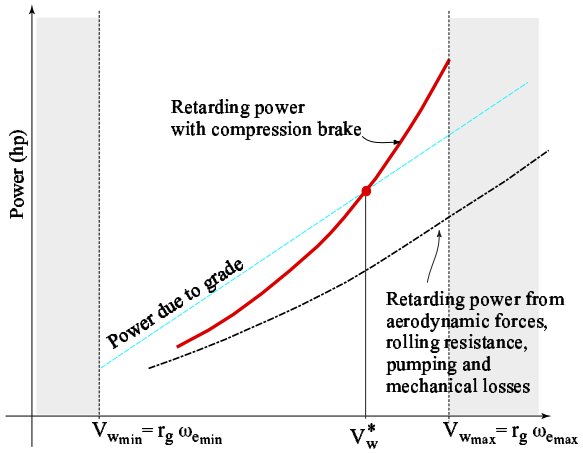

Figure 3: Vehicle braking power versus speed during a descent.

Fig. 2 and 3 are very informative and have extensively been used for actuator component design. However, the figures only show static behavior, hence, they do not provide any information of the transient behavior of the system. The brake valve timing affects both the maximum braking effort and the speed at which this maximum effort is achieved. The delays and time constants of the brake actuators, coupled with the dynamic response of the turbocharged engine, can impose severe limitations on the stability of the vehicle velocity. Nowadays, these limitations are primarily treated by predictive action of trained drivers. Identifying the bandwidth of the compression brake for different engine and drivetrain operating conditions is important for the design of safer and faster commercial heavy vehicles.

2. VEHICLE MODEL

A lumped parameter approximation of the vehicle rotational dynamics shown in Figure 4 can be used to describe the vehicle longitudinal dynamics during compression braking:

$$J_T \frac{d\omega_e}{dt} = TQ_{eb} + r_g(F_\beta - F_r - F_{qdr} - F_{sb}), \qquad (1)$$

where ω_e is the engine rotational speed, J_T is the total vehicle inertia reflected to the engine shaft, $F_\beta = Mg\sin(\beta)$ is the force due to road grade, β, and $F_r = \mu Mg\cos(\beta)$ is

the rolling resistance due to the tire-pavement interface coefficient, μ. Furthermore, $F_{qdr} = CV_w^2$ is the force due to friction, aerodynamic resistance, and other quadratic resistive terms. Finally, TQ_{eb} is the engine torque absorbed from the shaft during compression braking and F_{sb} is the friction brake force applied on the wheel rim. The total gear ratio $r_g = \frac{r_w}{g_t g_{fd}}$ includes the transmission and final drive gear ratio, g_t, and g_{fd}, respectively, and the wheel diameter, r_w.

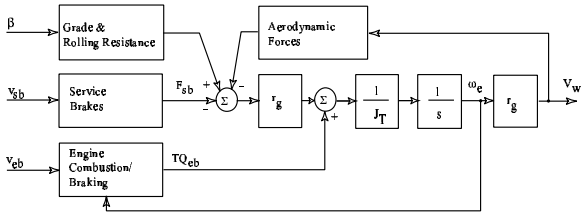

Figure 4: Open loop block diagram of the vehicle model.

The conventional friction brake force on the wheel can be modeled using a static nonlinear function of the applied pedal force, or simpler, the pedal displacement, v_{sb}, (for details see [4, 12, 14]), and a first order differential equation with a time constant, τ_{sb}, and a delay, t_{sb}, that are nonlinear and uncertain functions of temperature and brake conditions.

$$\frac{dF_{sb}}{dt}(t + t_{sb}) = \frac{1}{\tau_{sb}}(F^*_{sb} - F_{sb}(t + t_{sb})) \quad (2)$$

$$F^*_{sb} = f_{sb}(v_{sb}). \quad (3)$$

It is well known that the service brakes have weak DC authority because of overheating. The current practice of "snubbing" the service brakes (application of high pressure pulses) rather than "dragging" (application of a constant low pressure) exemplifies their low DC authority [3]. On the other hand, the compression brake is a powerful actuator in steady-state with unknown bandwidth. Its steady-state retarding ability is maintained for long periods due to the heat dissipation through the engine cooling system. Identifying the bandwidth of the compression brake for different engine and drivetrain operating conditions, requires a detailed crank angle based engine model. The compression brake torque on the crankshaft, TQ_{eb}, can be calculated using a static nonlinear function of engine variables and a first order differential equation with a time constant, τ_{eb}, and a delay, t_{eb}.

$$\frac{dTQ_{eb}}{dt}(t + t_{eb}) = \frac{1}{\tau_{eb}}(TQ^*_{eb} - TQ_{eb}(t + t_{eb})) \quad (4)$$

$$TQ^*_{eb} = f_{eb}(\omega_e, v_{eb}) \quad (5)$$

$$\begin{bmatrix} t_{eb} \\ \tau_{eb} \end{bmatrix} = \begin{bmatrix} f_{ebt} \\ f_{eb\tau} \end{bmatrix} (\omega_e, v_{eb}). \quad (6)$$

The static nonlinear brake torque, TQ^*_{eb}, is a function of engine speed, ω_e, and the brake valve opening, v_{eb}. The time constant, τ_{sb}, and the delay, t_{sb}, also depends on the engine speed and the brake valve opening.

Based on simulation of the crank angle based model (see Section 7., Fig. 18) we characterize the variable compression brake torque model (see Section 8.). The results agree with the existing steady-state data in literature [6, 7, 8]. Specifically, increased engine or turbocharger speed increases the braking torque and, more importantly, it affects the time constant of the braking actuator (i.e., how fast the actuator becomes effective). Boost pressure affects positively the braking torque. Last but not least, brake valve timing affects the braking torque. The crank angle model developed below allow us to understand the intricate dynamic phenomena during the transition from combustion to braking.

3. CRANK ANGLE BASED MODEL

Evaluation of the dynamic system response requires an accurate yet simple model of the cylinder-to-cylinder gas exchange process and combustion. During compression, the working fluid is the air (no combustion), therefore, thermodynamic models are generally accurate. In the following sections we document the mathematical model that describes the engine operation during combustion mode (dashed line in Fig. 2), during braking mode (solid line in Fig. 2), and during transition from one mode to the other. We also consider the engine response to changes in crankshaft speed and brake valve timing. Analysis of the braking effort for changes in valve timing sheds light into a variable retarding mechanism that potentially can be integrated with the service brakes.

The inputs to the model are: (i) fuel flow, (ii) engine speed, and (iii) brake valve timing (fixed duration and profile). The model is capable of representing transitions from combustion to braking by cutting-off the fuel injection and initiating the brake event. The crank angle representation allows us to capture the cylinder-to-cylinder interactions and the in-cylinder pressures that dictate the dynamic phenomena during the transition from combustion to braking. Based on the crank angle based model, we derive a mean-value representation of both the steady-state and the dynamic characteristics of the compression brake mechanism. The mean-value representation is used for control design and integration with the vehicle dynamics and service brakes. Further control development will be tested on the crank angle based model.

The nonlinear dynamic engine model consists of static elements (described by empirical equations), and dynamic elements (described by physically based equations). The parameters of the nonlinear static relations are determined by regression analysis of data collected from an experimental engine equipped with a compression brake mechanism. The simulation model is implemented on a Simulink/Matlab environment using C-coded S-functions.

3.1. STATE EQUATIONS, PLENUMS

The intake and exhaust manifolds and cylinders are modeled as plenums with homogeneous pressure and temperature distributions. The plenum model is based on the principles of the conservation of mass and energy, and the assumption of the ideal gas law, $pV = mRT$.

To summarize our notation, masses are defined by m, pressures, p, temperatures, T, flows, W, efficiencies, η, powers, P, volumes, V. We use the subscript c for compressor, t for turbine, i for the intake manifold, e_f, e_r, and e_c for the front, rear, and collector exhaust manifold, respectively. For cylinder j, we use cyl_j, where $j = 1 \ldots 6$. The flow from control volume x to control volume y is denoted by W_{xy}.

The gas properties in the intake manifold and the rear, front and collector exhaust manifolds are represented by two states: mass (m_i, m_{ef}, m_{er}, and m_e in kg), and pressure (p_i, p_{e_f}, p_{e_r}, and p_{e_c} in kPa). See Fig. 5 for a schematic of the engine and definitions of the plenums. The equations for the gas filling dynamics are derived on the basis of the total gas mass balances and the ideal gas law:

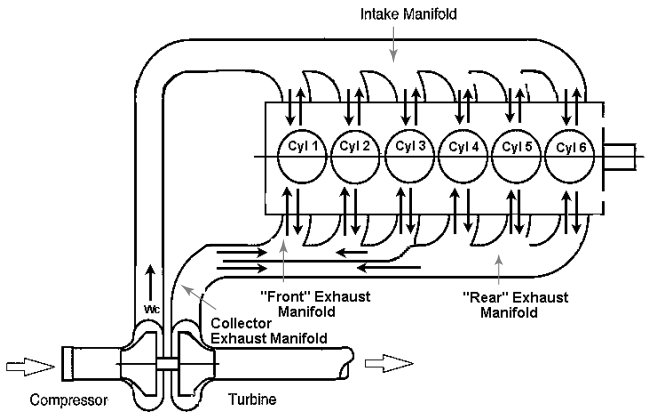

Figure 5: Schematic drawing of the engine and its control volumes.

$$\frac{dm_i}{dt} = W_c - \sum_{j=1}^{n} W_{icyl_j} + \sum_{j=1}^{n} W_{cyl_j i} \quad (7)$$

$$\frac{dp_i}{dt} = \frac{R}{V_i}\left[T_c W_c - T_i \sum_{j=1}^{n} W_{icyl_j} + T_{cyl_j} \sum_{j=1}^{n} W_{cyl_j i}\right] \quad (8)$$

where W_c and T_c are the compressor mass flow (kg/s) and temperature (K), respectively (see Section 3.4.). W_{icyl_j} is the mass air flow (kg/s) from the intake manifold into cylinder j, while $W_{cyl_j i}$ is the backflow (kg/s) from cylinder j into the intake manifold (see Section 3.3.). T_i and T_{cyl_j} are the intake manifold temperature (K) and the temperature for cylinder j, respectively. The temperatures are calculated based on the ideal gas law and the mass and pressure states in these control volumes.

Similarly, the state equations for the front exhaust manifold dynamics describe the rate of change of mass, m_{e_f}, and pressure, p_{e_f}, for that plenum.

$$\frac{dm_{e_f}}{dt} = \sum_{j=1}^{3} W_{cyl_j e_f} - \sum_{j=1}^{3} W_{e_f cyl_j} - W_t \quad (9)$$

$$\frac{dp_{e_f}}{dt} = \frac{R}{V_{e_f}}\left[\sum_{j=1}^{3} T_{cyl_j} W_{cyl_j e_f} - \sum_{j=1}^{3} T_{e_f} W_{e_f cyl_j} - T_{e_f} W_{e_f e_c}\right], \quad (10)$$

where $W_{cyl_j e_f}$ is the mass air flow (kg/s) out of cylinder j into the front exhaust manifold. This flow is calculated based on the flow through restriction equations (see Section 3.2.) and a constant orifice equation based on geometric data. Furthermore, W_t is the turbine mass flow (kg/s) (see Section 3.4.), V_{ef} is the exhaust manifold volume (m^3), and T_{ef} is the front exhaust manifold temperature (K). The state equations for the rear exhaust manifold mirror the equations for the front manifold directly. The state equations for the exhaust collector manifold, on the other hand, are given by:

$$\frac{dm_{e_c}}{dt} = W_{e_f e_c} - W_{e_c e_f} + W_{e_r e_c} - W_{e_c e_r} - W_t \quad (11)$$

$$\frac{dp_{e_c}}{dt} = \frac{R}{V_{e_c}}\left[T_{e_f} W_{e_f e_c} - T_{e_c} W_{e_c e_f} + T_{e_r} W_{e_r e_c} - T_{e_c} W_{e_c e_r} - T_{e_c} W_t\right], \quad (12)$$

where W_t is the flow through the turbine (kg/s).

The state equations for the cylinder states, mass, m_{cyl_j}, and pressure, p_{cyl_j}, include the time varying cylinder volume, V_{cyl_j} and a heat transfer and release description.

$$\frac{dm_{cyl_j}}{dt} = W_{icyl_j} - W_{cyl_j i} - W_{cyl_j e} + W_{ecyl_j} \quad (13)$$

$$\frac{dp_{cyl_j}}{dt} = \frac{\gamma}{V_{cyl_j}}\left(RT_i W_{icyl_j} - RT_{cyl_j} W_{cyl_j i} - RT_{cyl_j} W_{cyl_j e} + RT_e W_{ecyl_j} - \dot{V}_{cyl_j} p_{cyl_j}\right) + \frac{\gamma - 1}{V_{cyl_j}} W_{afb_j} Q_{lhv}, \quad (14)$$

where we, for simplicity, have coupled the front, e_f, and the rear, e_r, exhaust manifold into one variable, e. We calculate the released heat based on the apparent fuel burn rate, W_{afb} (kg/s), and the lower heating value of light duty diesel fuel, Q_{lhv}, (J/kg). In the calculation of W_{afb}, we have coupled the heat transfer. Thus, the integral of the apparent fuel burnt rate over a cycle is less that the

averaged mass fuel injected, v_f.

$$W_{afb_j} Q_{lhv} = W_{fb_j} Q_{lhv} + Q_{ht} \quad (15)$$

$$\int_0^{\Delta T} W_{afb_j} dt < v_f \Delta T, \quad (16)$$

where Q_{ht} is the heat transfer, and v_f is the cycle (ΔT) averaged fuel flow (kg/s). The fuel burn rate, W_{fb}, is calculated using the Wiebe approximation of the heat released during the premixed and the diffusion period of the combustion (see Section 4.).

The cylinder volume, V_{cyl_j}, (m^3) is a functions of the crank angle (θ):

$$V_{cyl_j} = V_{cl}\left[1 + \frac{1}{2}(rc-1)\left(R_r + 1 - \cos\theta_j - \sqrt{R_r^2 - \sin^2\theta_j}\right)\right] \quad (17)$$

$$\theta_j = \left(\frac{N_e}{60} 360 \cdot t + 120 \cdot j\right) \bmod 720^o, \quad (18)$$

where V_{cd} is the maximum cylinder displacement volume (m^3), V_{cl} is the cylinder clearance volume (m^3), and N_e is the engine speed in RPM. The engine has six cylinders, and therefore, a separation of 120 degrees between each cylinder, expressed by $120 \cdot j$.

3.2. FLOW THROUGH RESTRICTION

A quasi-steady model of flow through an orifice is used to derive the mass air flow through all of the exhaust restrictions and the cylinder valves. The quasi-steady relation of the air flow through a restriction is based on the assumptions of one-dimensional, steady, compressible flow of an ideal gas [5, 11]:

$$W = C_d A_v \Psi(p_d, p_u, T_u), \quad (19)$$

where W is the general mass air flow (kg/s), C_d is the discharge coefficient, A_v is the flow area function for the valve, and $C_d A_v$ is the effective flow area for the valve. The term Ψ is the standard orifice flow function that depends on the downstream pressure and temperature, p_d, and T_d and upstream pressure and temperature, p_u and T_u:

$$\Psi(p_d, p_u, T_u) = \begin{cases} \frac{p_u}{\sqrt{RT_u}} \Psi_o\left(\frac{p_d}{p_u}\right) & \text{if } p_d \le p_u \\ 0 & \text{if } p_d > p_u, \end{cases} \quad (20)$$

with

$$\Psi_o(x) = \begin{cases} \gamma^{\frac{1}{2}} \left(\frac{2}{\gamma+1}\right)^{\frac{\gamma+1}{2(\gamma-1)}} & \text{if } x \le c_r \\ x^{\frac{1}{\gamma}} \sqrt{\frac{2\gamma}{\gamma-1}(1 - x^{\frac{\gamma-1}{\gamma}})} & \text{if } x > c_r, \end{cases} \quad (21)$$

where $c_r = \left(\frac{2}{\gamma+1}\right)^{\frac{\gamma}{\gamma-1}}$ is the critical pressure ratio across the orifice.

3.3. VALVE FLOW

The mass air flow from the intake manifold into cylinder j, W_{icyl_j}, is calculated using previous Eq. 19-21:

$$W_{icyl_j} = f_{iv}\left(l_{iv}(\theta)\right) \cdot \Psi(p_{cyl_j}, p_1, T_1). \quad (22)$$

The effective flow area through the intake valve, $f_{iv} = C_d A_{iv}$, is calculated using crank angle data of the intake valve lift, $l_{iv}(\theta)$. Both maps are given by the engine manufacturer.

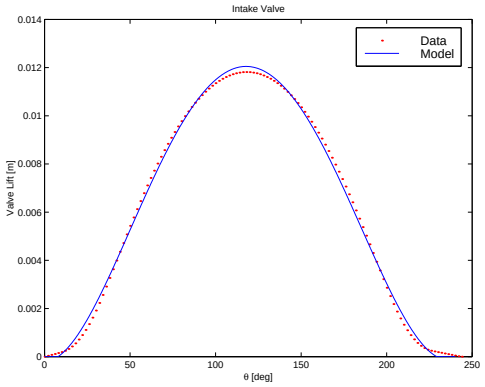

Figure 6: The intake valve lift versus crank angle.

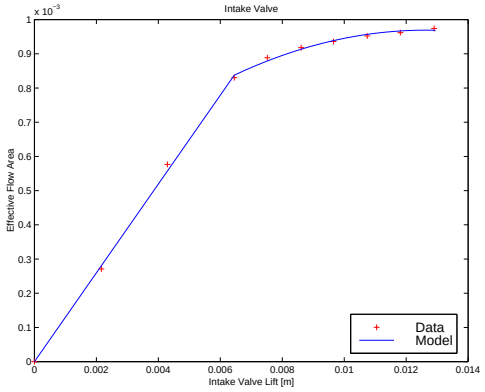

Figure 7: The intake effective flow area versus valve lift.

Similarly, the flow through the exhaust valve is given by:

$$W_{cyl_j e} = f_{ev}\left(l_{ev}(\theta)\right) \cdot \Psi(p_e, p_{cyl_j}, T_{cyl_j}), \quad (23)$$

where the exhaust valve map $f_{ev} = C_d A_{ev}$ is a function of the exhaust valve lift map, l_{ev}, and is provided by the engine manufacturer.

The brake valve is, technically speaking, the same as the exhaust valve. The only difference is the valve lift profile. This means that the flow through the brake valve is given by Eq. 23, where $l_{ev}(\theta)$ is replaced by $l_{bv}(\theta, v_{eb})$. Again, this valve lift is provided by the engine manufacturer.

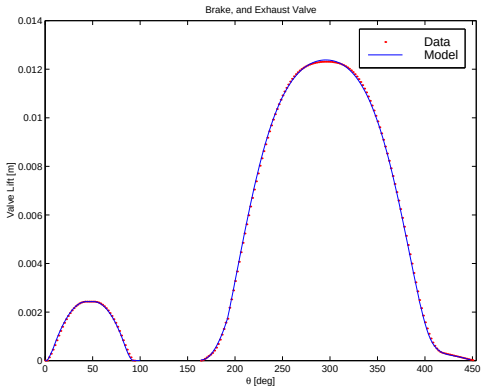

Figure 8: The exhaust and brake valve lift versus crank angle.

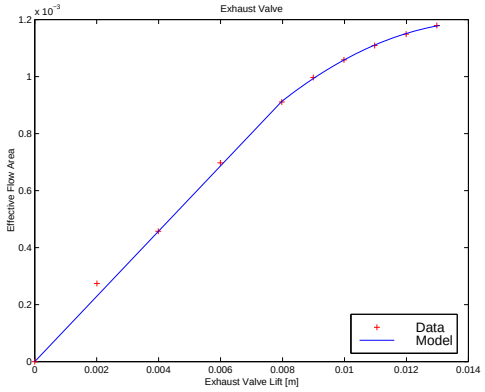

Figure 9: The effective flow area for both the exhaust valve and the brake valve versus valve lift.

3.4. TURBOCHARGER DYNAMICS

The turbocharger state equation consist of the rate of change of the turbocharger speed, N_{tc}, based on the conservation of energy on the turbocharger shaft:

$$\frac{dN_{tc}}{dt} = \frac{P_t - P_c}{I_{tc} N_{tc}}, \tag{24}$$

where P_t is the turbine power, P_c is the compressor power, and I_{tc} is the mass polar moment of inertia of the turbocharger. P_t and P_c are calculated based on an ideal adiabatic process, and steady-state data provided by the turbocharger manufacturer.

In particular, turbine maps, f_{t_w}, and f_{t_η} are used to determine the mass air flow, W_t and the efficiency, η_t. Both turbine maps are functions of turbocharger speed, N_{tc}, and pressure ratio, r_t, across the turbine.

$$P_t = W_t c_p \eta_t T_2 \left(1 - \frac{1}{r_t}^{\left(\frac{\gamma-1}{\gamma}\right)}\right) \tag{25}$$

$$W_t = f_{t_w}(N_{tc}, r_t) \tag{26}$$

$$\eta_t = f_{t_\eta}(N_{tc}, r_t) \tag{27}$$

$$r_t = \frac{p_2}{p_0},$$

where p_0 is the ambient pressure, and c_p is the specific heat capacity for constant pressure.

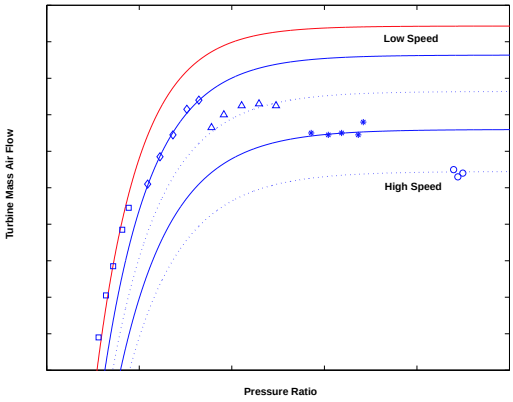

Figure 10: Map for turbine mass flow, W_t.

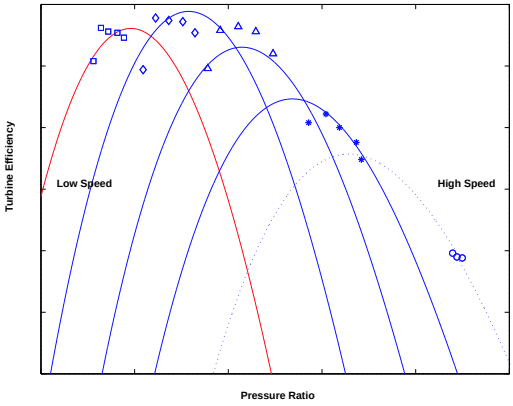

Figure 11: Map for turbine efficiency, η_t.

Similarly, using data from the compressor maps we obtain the compressor characteristics given in the following equations:

$$P_c = W_c T_0 \frac{c_p}{\eta_c}\left(r_c^{\left(\frac{\gamma-1}{\gamma}\right)} - 1\right) \tag{28}$$

$$W_c = f_{c_w}(N_{tc}, r_c) \tag{29}$$

$$\eta_c = f_{c_\eta}(N_{tc}, r_c) \tag{30}$$

$$r_c = \frac{p_1}{p_0}$$

where f_{c_w} is the compressor map for mass flow, and f_{c_η} is the map for the compressor efficiency, η_c. Both of these maps are functions of turbocharger speed, N_{tc}, and pressure ratio, r_c, across the compressor.

4. APPARENT FUEL BURN RATE

The apparent fuel burn rate is identified based on cylinder pressure data and modification of Eq. 14 for zero

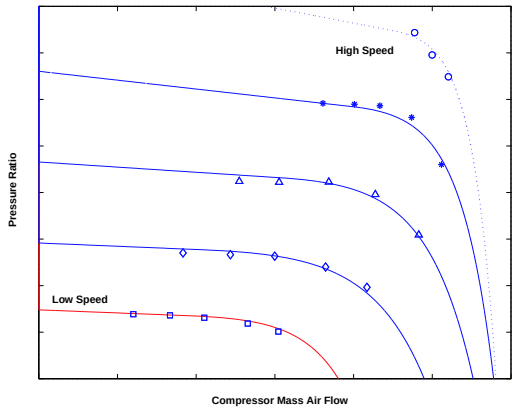

Figure 12: Map for compressor mass air flow, W_c.

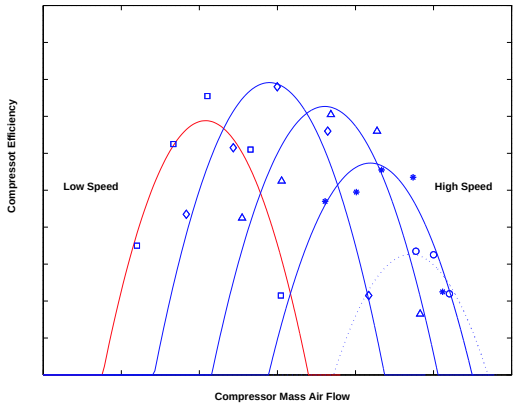

Figure 13: Map for compressor efficiency, η_t.

flow into and out of the cylinder:

$$W_{afb} = \frac{1}{Q_{lhv}(\gamma - 1)} \left(\gamma p_{cyl} \frac{dV_{cyl}}{dt} + V_{cyl} \frac{dp_{cyl}}{dt} \right). \quad (31)$$

We assume here that heat capacities are constant and couple the heat transfer to the calculation of an effective or apparent fuel burn rate. We stress that the apparent fuel burn rate we calculate in Eq. 31 is less than the actual fuel burn rate because we for simplicity assumed zero heat losses.

The apparent fuel burn rate curves for ten speed and load points are used to develop a crank angle functional approximation. Two Wiebe basis function have been combined to capture the premixed and the diffusion burning:

$$W_{afb} = max\left(W^d_{afb}, W^p_{afb}\right) \quad (32)$$

$$W^d_{afb} = C_d k_{d2} \left(k_{d1}+1\right) \theta_d^{k_{d1}} \exp\left(-k_{d2}\theta_d^{(k_{d1}+1)}\right) \quad (33)$$

$$W^p_{afb} = C_p k_{p2} k_{p1} \left(1-\theta_p^{k_{p1}}\right)^{(k_{p2}-1)} \theta_p^{(k_{p1}+1)}, \quad (34)$$

The variables $\theta_d = \frac{\theta - \theta_{soc}}{\Delta\theta_d}$ and $\theta_p = \frac{\theta - \theta_{soc}}{\Delta\theta_p}$ are defined over the diffused combustion duration, $\Delta\theta_d$, and the premixed combustion duration, $\Delta\theta_p$, respectively. To simplify the data fitting, we assume that both premixed and diffused-based combustion start at the same time, i.e., at start of combustion, θ_{soc}. Using the max function in the combination of the two curves in Eq. 32 resolves the two distinct starts for premixed and diffused-based combustion, as shown in Fig. 14. The start of combustion is computed

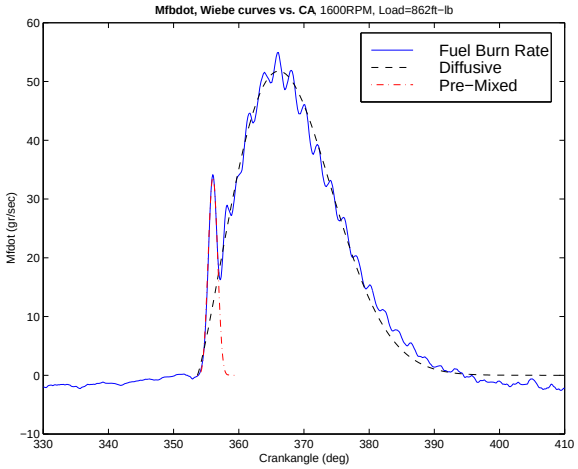

Figure 14: Combustion analysis and apparent fuel burn rate.

based on the start of injection θ_{soi} and the ignition delay $\Delta\theta_o$:

$$\theta_{soc} = \theta_{soi} + \Delta\theta_o \quad (35)$$

The six coefficients C's and k's, the two combustion mode durations, $\Delta\theta$'s, and the ignition delay $\Delta\theta_o$ are identified and regressed on fuel injected, v_f, and engine speed, N_e, using the ten available data points. A good compromise between data overfitting and small prediction errors is achieved with polynomials of second order in fuel flow and first order in engine speed for all variables.

The start of injection θ_{soi}, is also regressed based on fuel input and engine speed. Although, this does not give us the flexibility to use the injection timing as another model input, it allows us to maintain the simple combustion analysis in our model. The predicting ability of the developed model in fuel injection timing changes can be examined in future work.

5. SHAFT TORQUE

The torque produced at the crankshaft during combustion, or, transmitted from the crankshaft during braking, TQ_{cyl_j}, is calculated based on the individual cylinder pressure and piston motion using the idealized slider-crank mechanism [13]:

$$TQ_{cyl_j} = p_{cyl_j} \frac{\pi B^2}{4} r \sin(\theta_j) \left[1.0 + \frac{r}{R} \frac{\cos(\theta_j)}{\sqrt{1.0 - \left(\frac{r}{R}\sin(\theta_j)\right)^2}}\right] \quad (36)$$

where B is the cylinder bore (m^2), r is the crank radius (m), and L is the connecting rod (m).

The shaft torque is calculated by the summation of the individual cylinder torque. The average torque from the piston to the shaft during combustion is positive and the averaged torque from the shaft to the piston during braking is negative. Defining positive and negative torque allow us to seamlessly integrate the combustion mode and the braking mode and use the fuel flow and brake valve timing, $[v_f, v_{eb}]$ as one actuator (see Section 7., Fig. 22).

6. MODEL VALIDATION

Only steady-state data, collected in an engine-dynamometer facility are available for the experimental engine. Thus, we validate the steady-state cycle model behavior by comparing modeled and measured cylinder pressure. The validation plots during combustion mode and braking mode are shown in Fig. 15 and 16. The

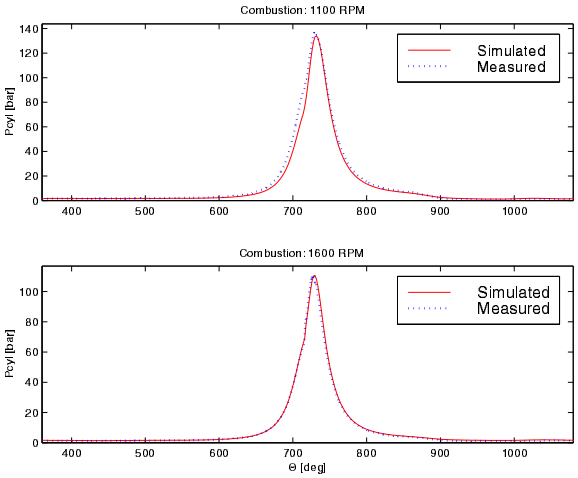

Figure 15: Comparison between the modeled and measured cylinder pressures for combustion operation.

mean-value prediction results are also compared with the engine data indicating less than ten per cent error in prediction of the steady-state behavior. Fig. 17 shows the predicted and measured power for the ten combustion data points we have, including maximum power for different engine speed (max power curve) and power for different fueling levels for $N_e = 1600$ RPM. The comparison of the engine retarding power (measured and predicted) for the nominal brake valve timing is also shown in Fig. 17 for different engine speed.

7. SIMULATION RESULTS

The engine model has been implemented in Matlab/Simulink with S-functions. It has 23 states with significantly different rates of convergence (stiff system) and multiple discontinuous functions that have been implemented with *if-then-else* statements. The stiffness and

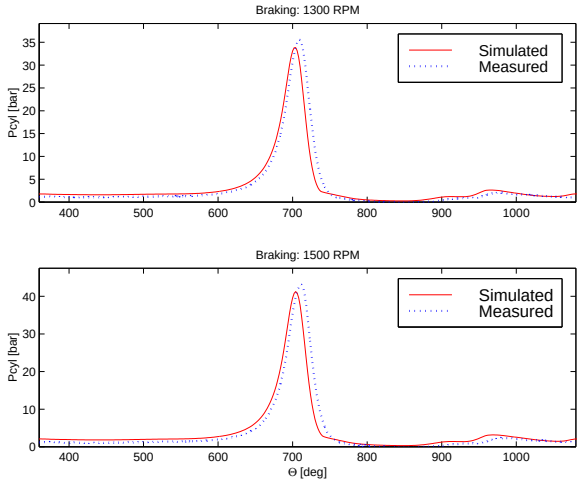

Figure 16: Comparison between the modeled and measured cylinder pressure for braking operation.

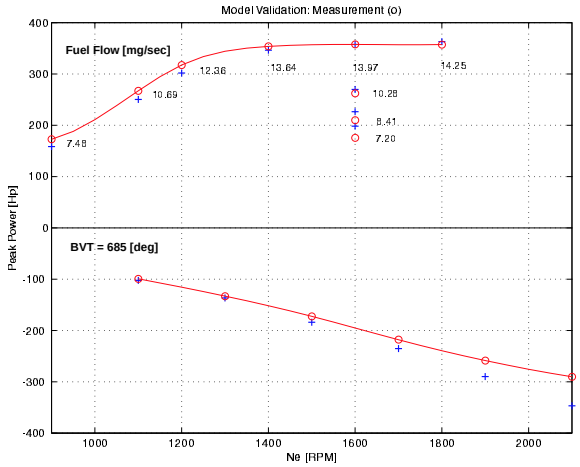

Figure 17: Comparison between predicted and measured mean-value shaft power.

discontinuity are handled satisfactory with the *ode23s* integration algorithm (one-step solver based on a modified Rosenbrock formula) within Matlab. Simulation of the engine model during a transition from combustion to braking is shown in Fig. 18. The simulation is performed at constant engine speed 1600 RPM as the first subplot on the left indicates. The last plot in the right column shows the fuel flow command. One can clearly see the fuel cutoff at the fifth cycle. At that point, the software is implemented to run with zero fuel (motoring) for one cycle before it opens the brake valve at 685 degrees. This brake valve command is shown in the last plot in the left column of Fig. 18. The model has been implemented with one cycle delay between the combustion and the braking mode to avoid extrapolation errors. It is shown that if we do not introduce this delay in the transition process the turbine efficiency drops below 0.2 which is outside the model region of validity. The delay can be viewed by observing

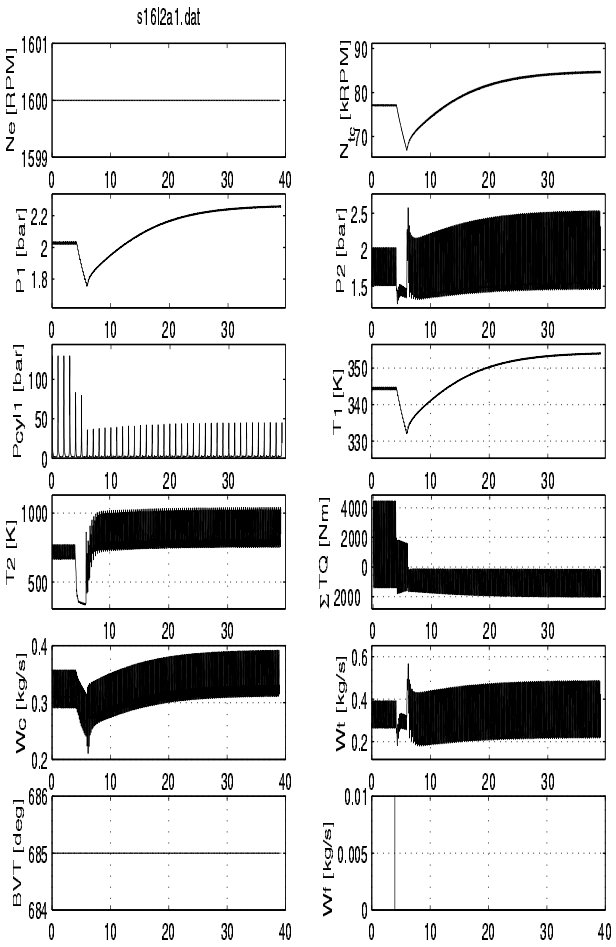

Figure 18: Simulation response during transition from combustion to braking.

the trace of cylinder pressure in the third plot of the left column.

The traces of intake and exhaust manifold pressure, as well as the turbocharger speed, demonstrate the importance of the turbocharger dynamics in predicting the transient torque response. The instantaneous torque response is shown in the fourth plot in the right column. One can see that the time necessary to transition from the steady-state combustion mode to steady-state braking mode is approximately equal to **ten cycles**. It is also evident that a first order lag will not be adequate to capture the mean-value behavior. Detailed analysis and signal processing of the simulation data follow in the next section. However, the above rough estimate of settling time indicates that the actuator dynamics will dominate the engine dynamics. Currently, the conventional devices have a fixed delay of 0.6 s, which is necessary to pump-up the system's hydraulic pressure sufficiently to open the brake valve against the high cylinder pressure. For comparison, we state here that conventional friction brakes that are pneumatically actuated, typically have 0.3 s delay, and a pneumatic pressure transient of 0.5 s.

The plots clearly show that interactions between the compression braking and the turbocharger dynamics are important to the retarding performance of the engine. Recent work by Hu et al. [6] emphasize the importance such interactions. Dynamic coupling between the compression effort and the turbocharger power determines the engine response during the transient operation of switching back to the conventional power generation mode. In [7], they report that the maximum turbocharger speed is lower during compression braking than it is during operation with combustion. On the other hand, the turbine accelerates faster during compression braking than during an increase in fuel level. Another intricate phenomenon arises during operation at high altitude [7]. Specifically, the turbine speed decays at high altitude instead of increasing, as occurs during normal engine operation. The coupling between the turbocharger and the engine dynamics is further augmented with transmission and driveline interactions which will be the subject of future work.

8. MODEL-ORDER REDUCTION

In this section we derive a series of local linear models of low order that capture the mean-value dynamic behavior of the engine. It is easy to see from Fig. 18 that the dominant dynamics are in the order of cycles and not in the order of crank angle. As a matter of fact, we would like to average all the quasi-period crank angle based dynamics. Analytically this can be done using singular perturbations, but such a rigorous treatment is not currently available. Developing such analytical techniques is an active research topic. Meanwhile, we can process simulation data using numerical techniques, such as signal processing and system identification tools. We perform here all the steps necessary to obtain a low order (3rd order) model from the original 23rd order that captures the dominant transient characterization. We call this process numerical model-order reduction (NMOR), as opposed to analytical model-order reduction (AMOR).

To develop an input-output model with brake valve timing, v_{eb}, and engine speed, N_e, as inputs and torque, TQ_{eb}, as output, we run the crank angle based model with small step changes in v_{eb} and N_e around a nominal point. The results are shown in Fig. 19. The third plot in Fig. 19 shows the event-averaged torque response. We obtain the cycle-averaged response by processing the crank angle torque output with a third order Butterworth filter with a cut-off frequency $\frac{1}{720}$ Hz. We then use the output error model (**oe**) in the identification toolbox in Matlab to estimate a low order model that can approximate the averaged output torque response (ΔTQ_{eb}) based on the v_{eb} step change (Δv_{eb}). Fig. 20 shows two different approximations, namely, a first order and a third order approximation. The third order one gives the best approximation, and, in fact, it is hard to distinguish it from the averaged torque trace. The third order transfer function

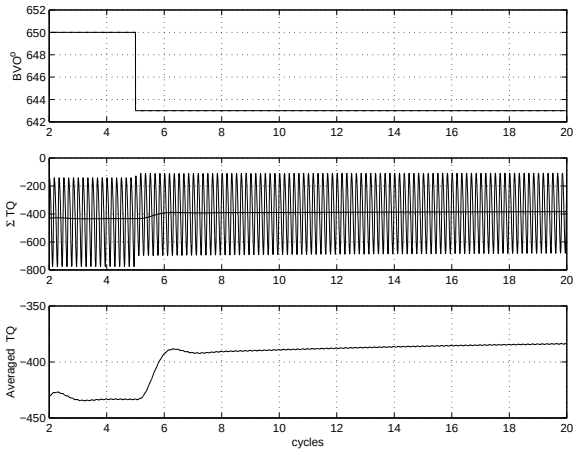

Figure 19: Simulation input/output data and lowpassed output.

is given by:

$$\frac{\Delta TQ_{eb}}{\Delta v_{eb}} = \frac{0.039s^2 - 9.631s - 12.82}{0.001s^3 + 0.0501s^2 + 1.7558s + 1.6417} \quad (37)$$

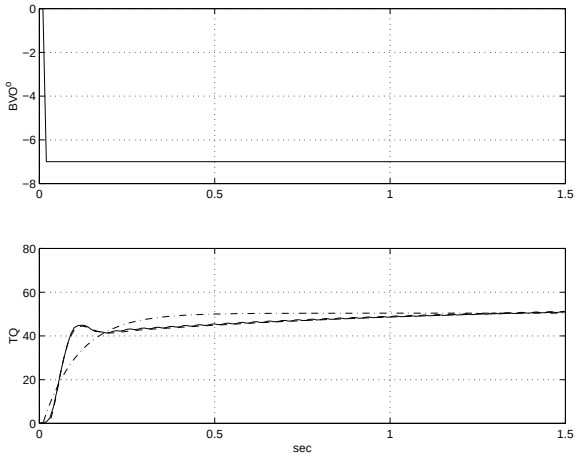

Figure 20: Prediction error estimate of an output-error model using a third order (dashed), and a first order (dashed-dotted) approximation.

By repeating the procedure with step changes in v_{eb} and N_e for several operational points, we obtain a family of linear third order models. Note here that a step up and a step down from the nominal point is required for the complete characterization of the nonlinear crank angle based model. Fig. 21 shows the Bode frequency response for the linear model for seven degrees step changes in brake valve timing up and down around $v_{eb} = 685^o$ for $N_e = 750$, 1500, and 2100 RPM. Similarly, we process simulation data for ten per cent step changes up and down around a nominal value for N_e, for fixed values of v_{eb} and fuel flow, v_f. We obtain low-order models and DC

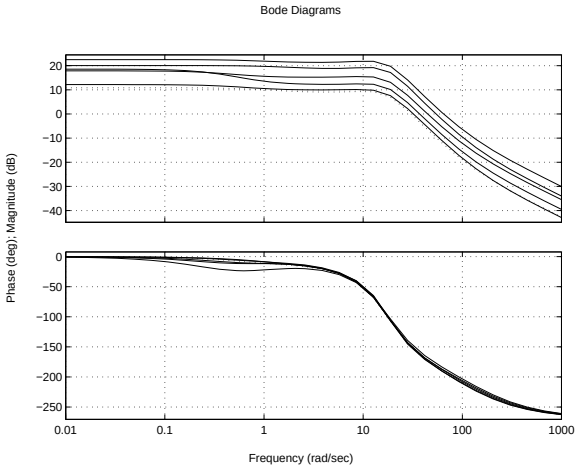

Figure 21: Bode frequency response of the reduced-order linear model.

values that we arrange in the plot shown in Fig. 22. Here, we have combined the fuel flow and the brake valve timing into one actuator, with positive values on the x axis representing fuel flow, and negative values representing brake valve timing. It is important here to note that the

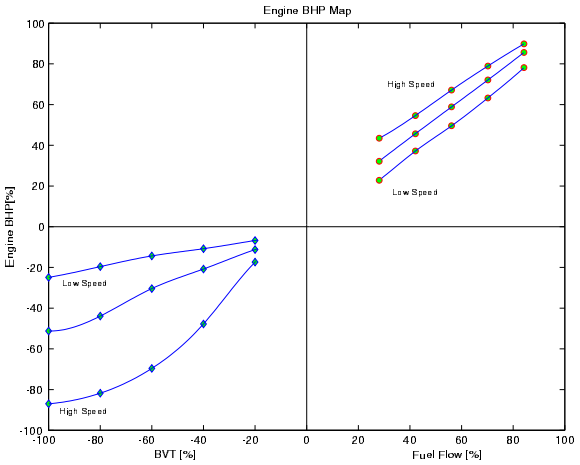

Figure 22: Generated and absorbed engine brake power plotted versus a unified engine actuator that combines the fuel flow, v_f, and the brake valve timing, v_{eb}, into one input signal.

control engineers are using similar techniques to develop control oriented models when experimental data are available from engine-dynamometer or vehicle testing. In our case, an engine with variable brake valve timing is still not available so we cannot collect data from an experimental engine. Thus, we use the physics-based crank angle model to acquire the necessary data. When the physical plant is still not available, physics-based models with minor calibration data can supply enough information for system analysis, feasibility studies, and actuator specification development for the initial component design [9].

9. CONCLUSION

The concept of variable valve timing, and its application to engine brake for commercial heavy vehicles are discussed in this paper. Conventional brake mechanisms have fixed brake valve timing and are typically used as on-off devices by experienced drivers. An engine retarder that allows variable braking power can be used in coordination with the service brakes to improve the vehicle longitudinal stability and controllability. To analyze and design such an advanced braking system, we first need to characterize the "new" braking actuator.

To be able to do so, we develop a crank angle based engine model that describes the intrinsic transient interactions between individual cylinder intake and exhaust gas processes, turbocharger dynamics, and vehicle dynamics during combustion and variable compression braking.

The model is fully dynamic and is calibrated using ten operating points. It is validated using quasi-static experimental data from an engine equipped with a conventional braking mechanism (fixed brake valve timing and fixed lift profile).

We modify the structure of the model by introducing variable brake valve timing (vary the timing with fixed lift profile). This allows us to use the engine as another full authority braking mechanism in vehicle speed and cruise control applications.

Finally, we perform numerical model-order reduction to obtain a family of low order linear models that can be used in control design and stability analysis. In future work, we will concentrate on control design and integration of the "new" variable compression brake with the service brakes for use in critical longitudinal maneuvers [10].

ACKNOWLEDGMENTS

This work is supported by the California Department of Transportation through the California PATH Program under MOU 372. Matching funds are provided by Mack Trucks, Inc.

CONTACT

Lasse Moklegaard, Department of Mechanical and Environmental Engineering, Engineering Building II, Room 1171, University of California, Santa Barbara, CA 93106-5070, lasse@engineering.ucsb.edu, Tel.: (805)893-7849, Fax: (805)893-8651.

REFERENCES

1. G. L. Borman and K. W. Ragland, *Combustion Engineering*, McGraw-Hill, 1998.

2. D. D. Cummins, "The Jacobs Engine Brake Application and Performance,", SAE Paper No. 660740.

3. J. W. Fitch, *Motor Truck Engineering Handbook,*, SAE Inc., 1994.

4. C. J. Gerdes, S. A. Brown, and K. J. Hedrick, "Brake System Modeling for Vehicle Control," Advanced Automotive Technologies - 1995 ASME IMECE, pp.105-112, 1995.

5. J. B. Heywood, *Internal Combustion Engine Fundamentals,* McGraw-Hill, 1988.

6. H. Hu, M. A. Israel, and J. M. Vorih, "Variable Valve Actuation and Diesel Engine Retarding Performance," SAE Paper No. 970342.

7. M. A. Israel and H. Hu, "Impact of Ambient Parameter on Operating Efficiency of Compression Release Engine Retarder Systems on Heavy Duty Diesel Engines," SAE Paper No. 932972.

8. Z. Meistrick, "Jacobs New Engine Brake Technology," SAE Paper No. 922448.

9. L. Moklegaard, A. Stefanopoulou, J. Schmidt, "Braking Control for Heavy Duty-vehicles," NSF Workshop on the Integration of Modeling and Control for Automotive Systems, Santa Barbara, 1999.

10. L. Moklegaard, A. Stefanopoulou, "Compression Braking Control for Heavy-Duty Commercial Vehicles," submitted to 2000 American Control Conference.

11. J. M. Novak, "Simulation of the Breathing Process and Air-Fuel Ratio Distribution Characteristics of Three-Valve, Stratified Charge Engines," SAE Paper No. 770881, 1977.

12. H. Raza, Z. Xu, and B. Yang, "Brake Modeling for AVCS Application," Report 94-01-01, 1994.

13. J. E. Shigley and J. J. Uicker, *Theory of Machines and Mechanisms*, 2nd Edition, McGraw-Hill, 1995.

14. D. Yanakiev and I. Kanelakopoulos, "Longitudinal Control of Automated CHV's with Significant Actuator Delays," Proc. 36th Confer. on Decision and Control, San Diego, 1997.